



1 Applying Deep Learning to NASA MODIS 2 Data to Create a Community Record of 3 Marine Low Cloud Mesoscale Morphology

4 Tianle Yuan^{1,2}, Hua Song³, Robert Wood⁴, Johannes Mohrmann⁴, Kerry Meyer¹, Lazaros
5 Oreopoulos¹, Steven Platnick¹

6 ¹Earth Science Directorate, NASA Goddard Space Flight Center

7 ²Joint Center for Earth Systems Technology, University of Maryland, Baltimore County

8 ³Science Systems and Applications, Inc.

9 ⁴Department of Atmospheric Sciences, University of Washington

10

11 Correspondence: tianle.yuan@nasa.gov

12

13 Abstract:

14

15 Marine low clouds display rich mesoscale morphological types, distinct spatial patterns of cloud
16 fields. Being able to differentiate low cloud morphology offers a tool for the research
17 community to go one step beyond bulk cloud statistics such as cloud fraction and advance the
18 understanding of low clouds. Here we report the progress of a NASA funded project that aims
19 to create an observational record of low cloud mesoscale morphology at a near-global (60S-
20 60N) scale. First, a training set is created by our team members manually labeling thousands of
21 mesoscale (128x128) MODIS scenes into six different categories: stratus, closed cellular
22 convection, disorganized convection, open cellular convection, clustered cumulus convection,
23 and suppressed cumulus convection. Then we train a deep convolutional neural network model
24 using this training set to classify individual MODIS scenes at 128x128 resolution, and test it on a
25 test set. The trained model achieves a cross-type average precision of about 93%. We apply the
26 trained model to 16 years of data over the Southeast Pacific. The resulting climatological
27 distribution of low cloud morphology types show both expected and unexpected features and
28 suggest promising potential for low cloud studies as a data product.

29

30 **1. Introduction**

31 Marine low clouds are important for the mass, heat, and momentum transport in the planetary
32 boundary layer (PBL) and between the PBL and free troposphere, the radiative energy balance
33 of the climate, and the magnitude of feedback strength under climate change. Observations of
34 marine low clouds are indispensable for advancing our understanding of these clouds for
35 deriving new theories and insights and for model validation and constraining. Modern satellite
36 observations have the advantage of providing global and long-term coverage. Current satellite
37 products offer detailed pixel-level retrievals of cloud properties such as cloud optical depth,
38 cloud droplet effective radius, and cloud phase. Most cloud classification schemes are based on
39 either single pixel measurements or joint-histogram of two cloud properties.

40



41 However, marine low clouds are known to have various mesoscale morphology types since first
42 satellite observations of clouds became available (Agee and Dowell, 1974). These mesoscale
43 morphology types are created by the characteristic patterns into which clouds are organized
44 (Figure 1). Cloud mesoscale morphology types are not only phenological classifications of
45 satellite images, but also manifestation of complex mixture of underlying physical processes
46 (Atkinson and Zhang, 1996; Stevens et al., 2005; Wang and Feingold, 2009; Wood, 2012; Wood
47 and Hartmann, 2006). These physical processes are critical for fundamental understanding and
48 better modeling of marine low clouds because of their impact on mass, heat, and momentum
49 transport, on radiative energy balance, and their feedbacks to climate change. Wood and
50 Hartmann (2006) trained a two-layer neural network on probability distribution functions and
51 2-d power spectra of liquid water path to classify cloud morphology into four categories for
52 256x256 scenes. The method has been successfully used to analyze morphology types and
53 associated cloud properties (McCoy et al., 2017; Muhlbauer et al., 2014).

54

55 Here we introduce a NASA funded project to classify marine low cloud observations into six
56 different mesoscale morphology types based directly on full images without engineering
57 features. The goal is to produce a community data record that spans about two decades at
58 near-global scales that will enable the research community to go beyond bulk cloud statistics
59 and will advance our understanding of low-level mesoscale convective clouds through
60 exploiting the rich spatial information content of observations. Section 2 describes the data and
61 methodology; section 3 introduces preliminary results and section 4 gives discussions of future
62 plan and outlook of the data product; section 5 concludes.

63

64 **2. Data and methods**

65

66 a. Data source

67 The primary observational data for this study are from the MODerate resolution Imaging
68 Spectrometer (MODIS) onboard the Aqua satellite. We use reflectance from channels 1
69 ($0.65\mu\text{m}$), 3 ($0.47\mu\text{m}$), and 4 ($0.55\mu\text{m}$) and cloud optical depth, cloud droplet effective radius,
70 cloud mask, and cloud top height from the MODIS cloud product (Platnick et al., 2016) in
71 building up the training set. The cloud optical depth and effective radius retrievals are
72 combined to produce cloud liquid water path (Platnick et al., 2016). Reflectance from channel 4
73 is used for deep neural network model training and inference, while the other MODIS
74 observations and products are used for data quality control, filtering, and contextual
75 information, as explained below.

76

77 We first break MODIS images into 128x128 scenes and filter out scenes that contain significant
78 fraction of high clouds (no more than 10%), defined as pixels with cloud top height above 6km,
79 or whose low cloud fraction is lower than 5%. We also exclude scenes whose viewing zenith
80 angle is greater than 45 degrees. Scenes with more than 10% land are also excluded. The
81 resulting scenes are treated as dominated by marine low clouds.

82

83 For training purpose, we create auxiliary images that contain the broad context of the scene of
84 interest and distributions of the liquid water path and cloud top height for the scene (Figure 2).



85 The scene image together with the auxiliary images are presented to a panel of human experts
86 on the Zooniverse platform (www.zooniverse.org) for manual labeling. We intend to use the
87 same platform in the future to crowdsource the labeling task.

88
89 Spatiotemporally collocated Modern-Era Retrospective analysis for Research and Applications,
90 version 2 (MERRA-2) (Gelaro et al., 2017) data is used to provide meteorological variables for
91 each scene.

92 93 b. Morphology types

94 Marine low cloud mesoscale morphology patterns are extremely diverse. In order to keep the
95 task manageable, we settle on six representative types to keep the task manageable. They are
96 stratus, closed cellular convection, disorganized cellular convection, open cellular convection,
97 clustered cumulus, and suppressed cumulus (Figure 3). These types are by no means exhaustive
98 given the diversity of observable patterns. However, these six types are the most common and
99 largely representative of the data when we inspect a large collection of scenes. We also believe
100 that these types have distinct underlying physical processes. Stratus is mostly created by
101 relatively uniform radiative cooling or driven by synoptic weather systems such as fronts while
102 closed cellular convection is driven by radiative cooling and organized into distinctive
103 honeycomb mesoscale patterns. Disorganized cellular convection is characterized by a
104 combination of elements of convection and large portion of stratiform clouds that tend to have
105 large droplet sizes and small cloud optical depths, creating their characteristic appearance.
106 Their cellular sizes are typically larger, on the order of 100km, compared to closed cellular
107 convection, on the order of 10km. Open cellular convection is characterized by cells that are
108 clear in the center and exhibit vigorous shallow convection around it. These convective clouds
109 are often precipitating based on satellite and ship-based observations, which is a likely driving
110 force that creates and maintains this mesoscale morphology type (Wang and Feingold, 2009).
111 Clustered cumulus convection is made up of shallow, vigorous convective elements that
112 aggregate together, accompanied by scattered shallower and optically thinner cumulus clouds
113 nearby. The suppressed cumulus type is dominated by individual, scattered cumulus clouds that
114 can sometimes have patterns like lines and branches.

115 116 c. Method

117 To illustrate the difficulty of classify morphology types using one-point statistics such as
118 histograms, we show the mean probability density functions (PDFs) of cloud optical depth and
119 droplet effective radius for each type in Figure 4. The significant overlap between PDFs of
120 different types makes it quite hard to classify the scenes based on these PDFs. On the other
121 hand, deep convolutional neural network (DCNN) models have been shown to separate
122 complex patterns into different categories at a human level (LeCun et al., 2015). We apply a
123 transfer learning approach to our classification task in a supervised fashion although separate
124 efforts of unsupervised training also seem promising (Yuan, 2019).

125
126 Specifically, we use a pretrained model (Simonyan & Zisserman, 2015) as a feature extractor
127 and fine-tune it with our training set. The pretrained model is a 16-layer DCNN that is trained
128 on the large-scale ImageNet dataset (Deng et al., 2009). Its weights are fixed. We add three



129 additional layers to the pretrained model, called VGG-16 and train the resulting full model on
130 our training set, the fine-tuning step. The output of the full DCNN model is a six-element
131 vector whose elements sum up to 1 and are interpreted as the probability that the model
132 assigns to one of the corresponding types. We assign every scene to the type that has the
133 highest probability and therefore effectively we have a metric to measure how confident the
134 model is for each classification, which provides useful information for users who may apply
135 filters to the data.

136

137 To build the training set, our team together with several expert level volunteers first manually
138 labeled thousands of scenes using the Zooniverse online tool. We retain only those scenes that
139 are unambiguously belonging to a certain type to present the best possible training set, which
140 includes hundreds of samples for each type. We augment the training set by rotating each
141 scene by 90 and 180 degrees and also flipping the open cellular scenes to increase their sample
142 size.

143

144 **3. Results**

145 Here we report results for the training, show the classification at work at a granule level and for
146 two typical low marine low cloud regimes: winter time mid-latitude region downwind of the
147 East Coast of US and Canada and sub-tropical Southeast Pacific region.

148

149 a. Training performance

150 The training asymptotically converges to a plateau in terms of accuracy pretty quickly, within
151 about 30 epochs (Figure 5). Around epoch 30, the validation accuracy reaches a maximum. The
152 training and validation accuracies are at around 98% and 93%. We save the model configuration
153 with the best validation accuracy. After training, the model is applied to a test set that it has
154 never seen before. The resulting confusion matrix is shown in Figure 6. The trained model
155 achieves an average precision of about 93% across different types. Open cellular and
156 disorganized cellular convection, are the two morphology types with the lowest accuracy
157 mainly because they had the lowest number of training samples. With further increase in
158 training samples in the future, we are confident that corresponding accuracies can be further
159 improved. The biggest challenge for the model comes from separating disorganized cellular,
160 open cellular, and clustered cumulus types. It is also worth noting that there is inherent
161 uncertainty with the classification since even expert labelers sometimes disagree on the same
162 scenes.

163

164 b. An example granule

165 An example of a classified MODIS granule is shown in Figure 7. The classification results are
166 overlaid on the visible MODIS image as colored circles whose position represents the center of
167 corresponding 128x128 scene. This is a low cloud dominated granule with a complex mix of
168 different morphology types. The few missing scenes within the viewing zenith angle limits are
169 due to subvisible high clouds overlapping the visible low clouds, which is not rare even for these
170 low cloud dominated regions (Yuan and Oreopoulos, 2013), as well as a couple of scenes with
171 too little low clouds. One can visually confirm that the model performs quite well in picking up
172 morphology types and their transitions corroborating the results in Figure 5.



173

174 c. Test run over the wintertime Northwest Atlantic

175 During the winter, there can be many cold air outbreak events over the Northwest Atlantic
176 region. They create maritime low cloud systems with various mesoscale morphology types. We
177 apply our model to data in winter of 2011. We first filter the raw data to include only marine
178 low cloud scenes using the criteria discussed in section 2. The 128x128 pixel scenes are fed into
179 the trained DCNN model for classification. For each scene, we record its morphology type,
180 geolocation, time and save the 2-D MODIS cloud retrieval parameters such as cloud optical
181 depth, cloud droplet effective radius, and cloud top pressure. In this run, we do not oversample
182 the data and therefore scenes do not overlap with each other.

183

184 Figure 8 shows frequency of occurrence maps for each cloud type along with surface wind
185 vectors. Stratus clouds dominate in the Hudson Bay and Labrador Sea. They also frequently
186 appear over waters around the Newfoundland and, to a lesser degree, along the east coast of
187 US and Canada. There is also a local maximum in the western part of the Gulf of Mexico. Closed
188 cellular type dominates the warm water of the Gulf Stream where cold continental air meets
189 the warm water, which induces large flux of moisture and heat from the ocean into the
190 boundary layer and gives rise to formation of low clouds. These low clouds mostly appear as the
191 closed cellular type according to MODIS. The disorganized type only appears in significant
192 quantity in the subtropics away from the coast. Open cellular clouds peak in the area south of
193 the Greenland and in the Labrador Sea and have a local maximum that is centered around
194 60°W and 35°N. Both are downwind of the closed cellular cloud peaks. The clustered and
195 suppressed cumulus clouds mostly occur in the subtropics and tropics.

196

197 d. Results over the Southeast Pacific region

198 We obtained all relevant Aqua MODIS level-1b and level-2 files for the Southeast Pacific region
199 (5°S-45°S, 70°W-125°W) between 2003 and 2018. The total volume of data is about 30 Tb. This
200 region is well known for the semi-permanent stratocumulus clouds.

201

202 Figure 9 shows the 16-year climatology of sea surface temperature (SST), estimated inversion
203 strength (EIS) (Wood and Bretherton, 2006), and frequency of occurrence maps for each
204 morphology type in the Southeast Pacific region. The frequency is normalized by the number of
205 total MODIS scenes, including both low cloud and non-low cloud ones.

206

207 Stratus clouds predominantly occur near coastal upwelling regions in the subtropics as well as
208 in the mid-latitude regions south of 40 degrees. Both features agree with our expectations.
209 Stratus can still occur in other parts of the domain, but with frequencies generally below 10%.
210 Their frequency significantly drops away from the local maxima in the mid-latitudes and along
211 the coast. The local maxima of stratus occurrence frequency coincide spatially with cold SST.

212

213 The closed cellular type occurs most frequently about five hundred kilometers away from the
214 coastlines. The absolute maximum is located around 27°S and 75°W, which is also where EIS
215 peaks. Indeed, the frequency of closed cellular type roughly correlates with the EIS pattern. The
216 frequency of this type drops off from its peak location more gradually compared to that of the



217 stratus. Its frequency is nevertheless below 10% west of 90°W and the direction of the
218 frequency of occurrence gradient is almost east to west. The location of peak frequency for the
219 disorganized type is further away from the coast and occurs around 21°S and 89°W. The
220 frequency map of this type also has an overall correlation with the EIS west of 90°W.

221
222 The frequency map for the open cellular type is the most distinct. Its peak features a bullseye
223 pattern and occurs further downwind of the peak of the disorganized type, with a peak
224 frequency of only about 10%. This type also appears relatively frequently in the mid-latitudes
225 associated with mid-latitude cyclones. Its spatial pattern has no direct correlation with either
226 EIS or SST patterns, possibly implying internal mechanisms that are responsible for their
227 appearances. Both the closed and open cellular locations agree qualitatively with the findings
228 from Wood and Hartmann (2006), although the addition of other cloud types resulted in lower
229 frequencies of these types in our dataset. It is also worth mentioning that the disorganized
230 cellular type has a different geographic occurrence when compared to Wood and Hartmann
231 (2006). This is because under that classification scheme, 'disorganized' includes the bulk of
232 scenes which we classify as suppressed and clustered; the more narrowly-defined disorganized
233 cellular type in our classification is geographically more closely associated with the other
234 cellular cloud types. The clustered cumulus type occurrence appears to have a general
235 anticorrelation with the EIS map. The suppressed cumulus type occurs most frequently in the
236 tropics where the SST is the warmest.

237

238 **4. Discussions and future work**

239 a. Notable new insights

240 Open cellular clouds are less prevalent than previously thought (Atkinson and Zhang, 1996;
241 McCoy et al., 2017; Muhlbauer et al., 2014), especially in subtropical regions. We attribute this
242 to the combination of advanced quantitative observation techniques developed here and the
243 delineation of clustered cumulus and open cellular types. The early studies did not have
244 comprehensive observations to rely on. The more recent results may have included the two
245 types together into the open cellular type, which overestimated the occurrence frequency of
246 the open cellular type in the subtropics. However, given the relatively minor presence of
247 clustered cumulus type in the midlatitudes, the open cellular type may indeed be quite
248 prevalent there, which agrees with previous studies.

249

250 There is a strong spatial correlation between both EIS and SST and the frequency of stratus in
251 two regions analyzed, especially north of 35°N, suggesting a strong control of atmospheric
252 stability and cold SST on this cloud type in higher latitude regions. Their control on other cloud
253 types may not be as tight given the loose spatial correspondence between both EIS and SST and
254 frequency of other cloud types, implying either other large-scale variables are in control or
255 internal cloud processes are more important. We will leave such explorations for future studies.

256

257 b. Expanding the scale of test runs and further analysis

258 We plan to expand the test run to near-global scales for about two years. These runs will
259 include time periods that overlap those of several field campaigns that have rich in-situ and
260 ground and airborne remote sensing data. Together with these datasets, the satellite product



261 will help to advance the understanding of low cloud mesoscale morphology. The global scale
262 will also allow us to examine the general distributions of morphology types and intercompare
263 the characteristics of low cloud morphology in different ocean basins. Further data analysis of
264 the current test run and future runs will target questions related to the variability of low cloud
265 morphology and its driving forces. We plan to release part or all of the test run results to beta
266 testers for feedback and test use from the community.

267

268 c. Collocating with other satellite sensors and meteorology

269 We plan to collocate each classified low cloud scene with data from sensors like CloudSat cloud
270 profiling radar, CALIOP lidar, the Advanced Microwave Scanning Radiometer for EOS (AMSR-E
271 and AMSR-2), and Atmospheric InfraRed Sounder (AIRS) as well as the MERRA-2 reanalysis
272 products. Such collocated set of variables will be useful to the research community for studying
273 the behavior of low cloud morphology under different environmental conditions

274

275 d. Further improvement of the model

276 The current model works pretty well overall, particularly for closed cellular, suppressed
277 cumulus and clustered cumulus types. However, there is room to improve for other types. We
278 target two fronts for improvement: improving the model itself and increasing the quality and
279 quantity of training data. For the former goal, we plan to test different pre-trained models and
280 what features to keep and how to best set up the classifier on top of these extracted feature
281 vectors. For the latter goal, we have developed analysis tools to help us understand the
282 agreement among human experts in the training set. This helps us to target types that need the
283 improvement. We will use the Zooniverse tool to achieve this. Further increase in training data
284 also allows us to better characterize the uncertainty in expert labeling of each category. We are
285 looking for expert level volunteers to join us to increase the training sample size.

286

287 e. Increasing the number of types

288 Some of the mesoscale types can be further divided into subtypes. For example, the frequency
289 of suppressed cumulus type is quite high in the low latitudes and based on the manual labeling
290 they could be further divided into multiple subtypes. We will explore the feasibility of this by
291 assessing resource constraints and the feedback from the community.

292

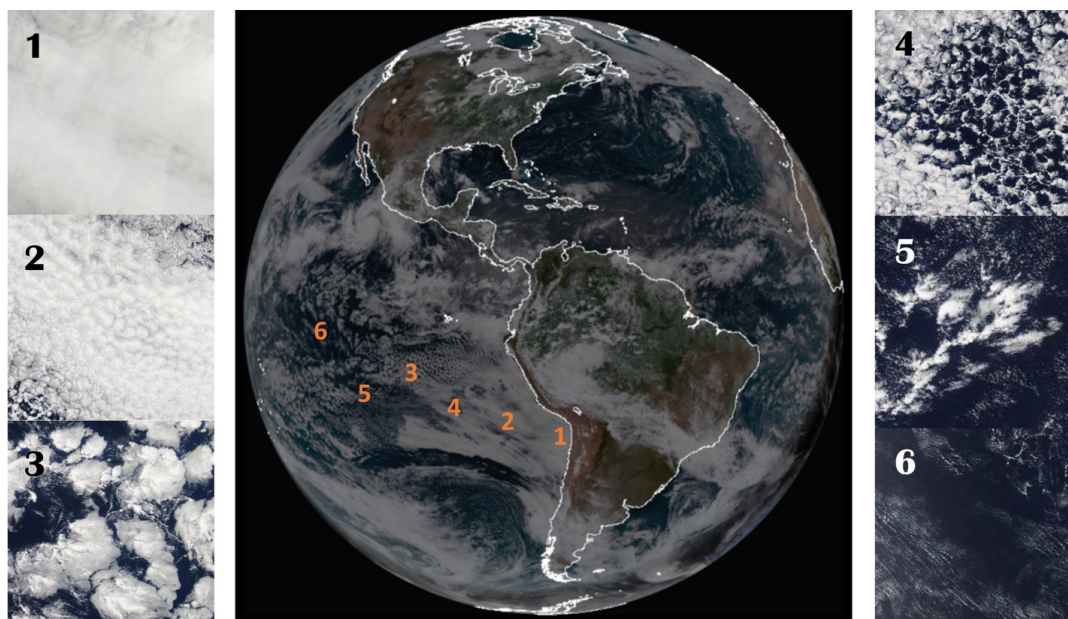
293

294 **5. Conclusions**

295 We have developed a working deep neural network model to automatically classify cloudy
296 scenes into six mesoscale morphology types. Initial test run results showed promising results
297 for the Southeast Pacific and Northwest Atlantic. Using the tool, we plan to extend the dataset
298 and create a community mesoscale morphology type product for low marine clouds observed
299 by MODIS. We will further develop the product and actively look forward to community
300 involvement such as beta testing, volunteering, and user feedback.

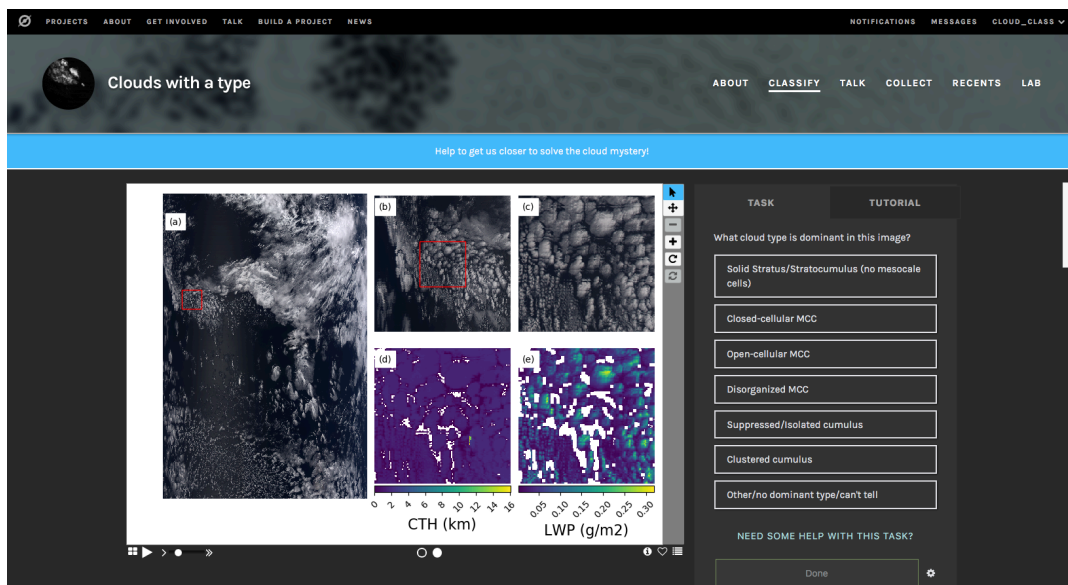
301

302



303
304
305
306
307
308
309

Figure 1: A full disk image of GOES-16 on Aug 6, 2018 and six scenes of MODIS images at smaller scales representing different morphology types at corresponding locations in the GOES image. Except scene 1, all scenes are from the same day. Scene 1 is from a different day because there was no representative stratus scenes on this day in the Southeast Pacific region.

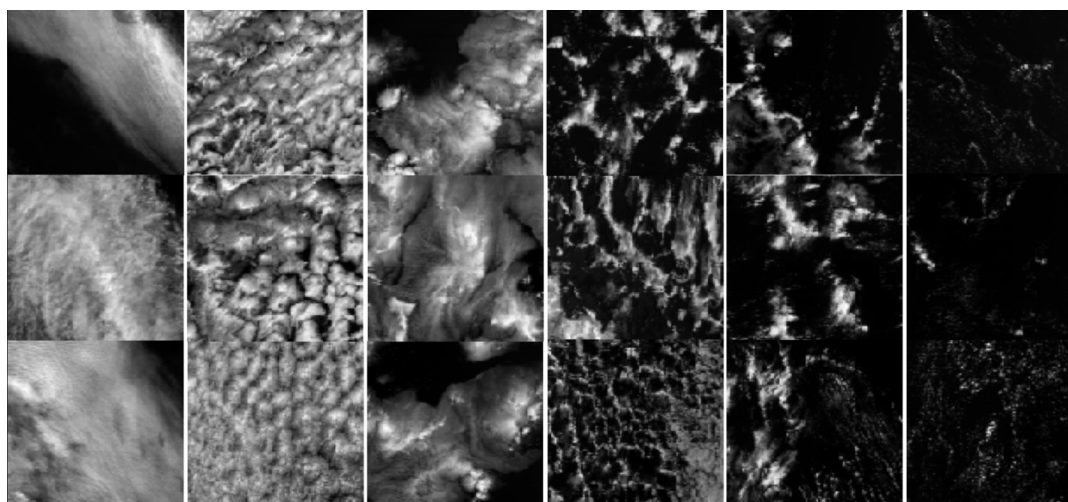


310
311
312

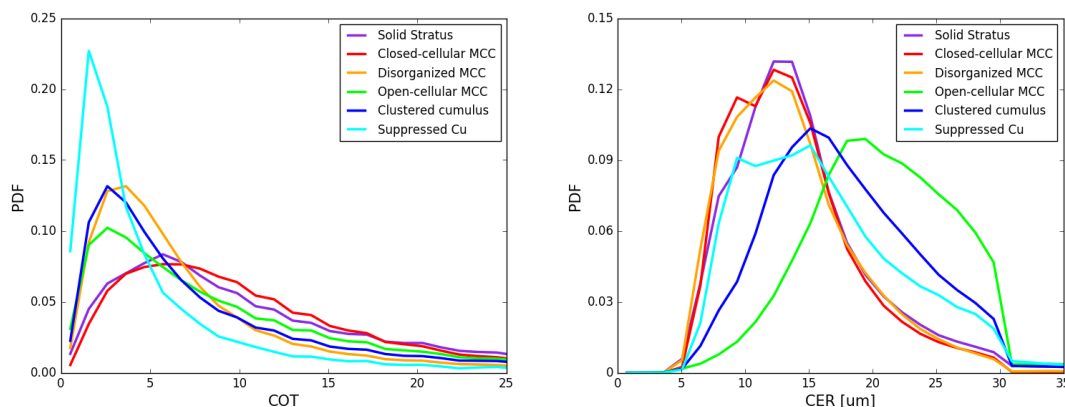
Figure 2: the Zooniverse interface for manual labelling. The center image is made up of five panels. Panel a shows the full granule (usually 2030x1350 pixels) true color image for large



313 context. Panel b shows a portion of the granule immediately surrounding the scene to be
314 labelled, outlined by the red square. Panel c shows the visible scene image while panels d and e
315 show the cloud top height and LWP fields in the scene to be labelled. The panels to the right of
316 the center image show labelling choices. The tutorial document is available by clicking on the
317 'FIELD GUIDE' tab on the right side. Additional options for scenes with heavily mixed types,
318 scenes with sea ice, or scenes with other issues are found in the 'other' menu. The image is a
319 screenshot of our Zooniverse project.
320
321



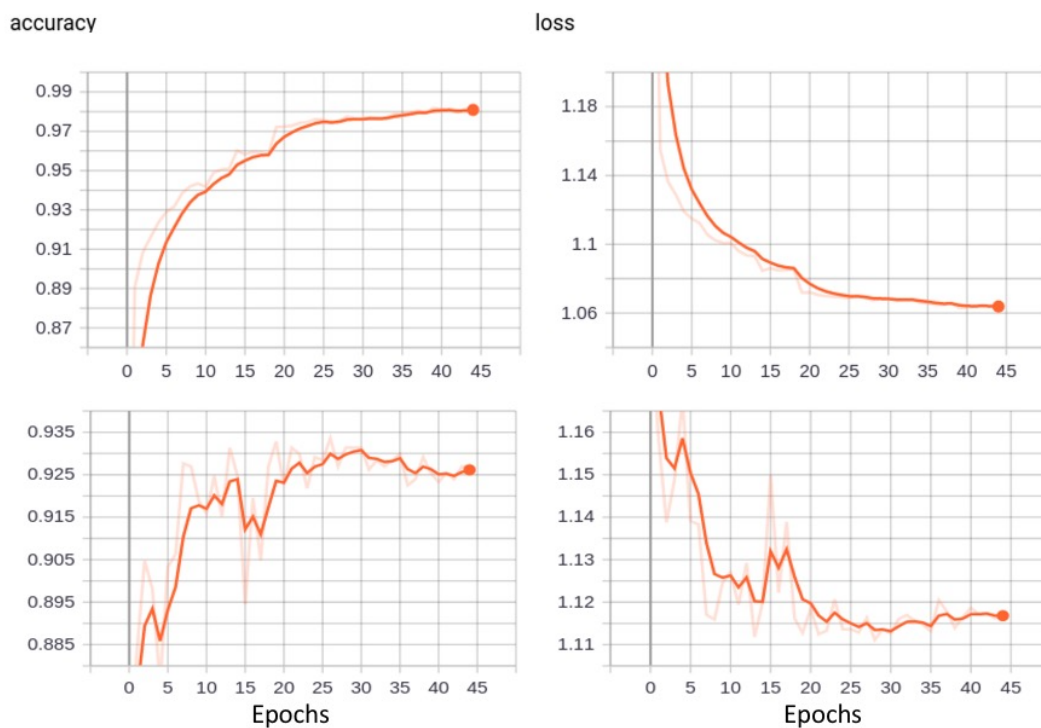
322
323
324 Figure 3: Example scenes of MODIS single channel images for the six different types. From left
325 to right: stratus, closed cellular, disorganized cellular, open cellular, clustered cumulus, and
326 suppressed cumulus types. Images taken by the NASA MODIS.
327



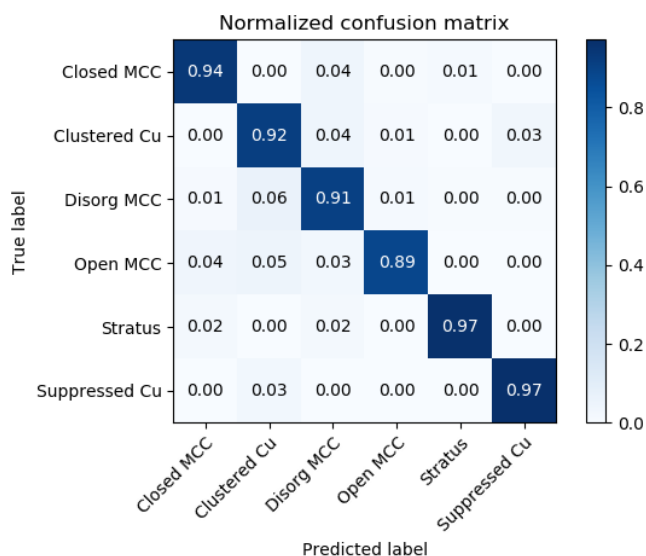
328
329
330 Figure 4: PDFs of cloud optical depth and cloud effective radius for six morphology types.
331 Significant overlaps are observed for PDFs of both variables among different morphology types.



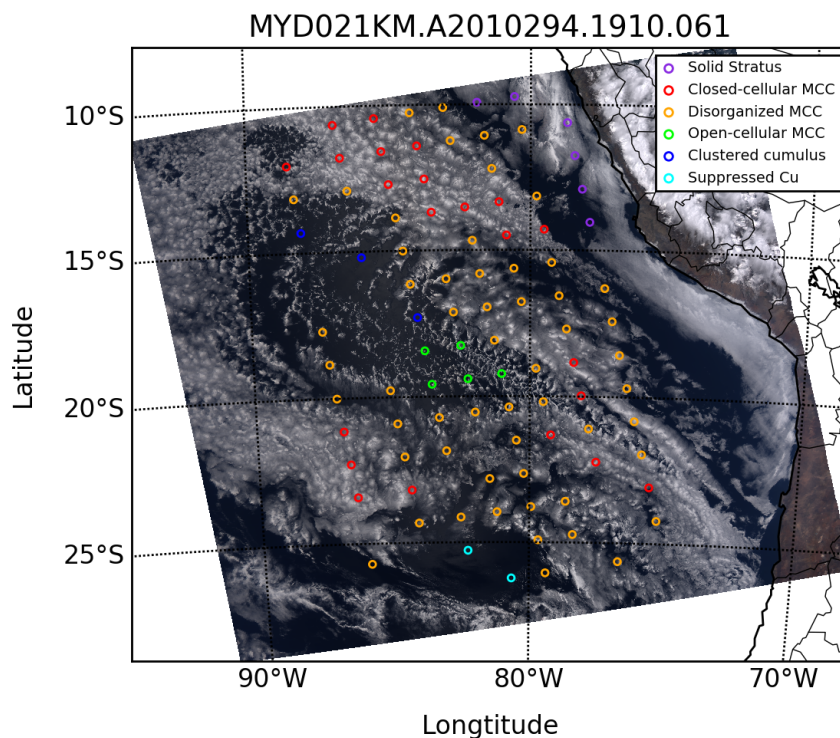
332
333



334
335 Figure 5: Training (upper two panels) and validation (lower ones) accuracy and loss trajectories.
336 By around epoch 30, the validation accuracy peaks while validation loss bottoms out and the
337 training loss and accuracy asymptotically reach their minimum and maximum, respectively,
338 which indicate further training may be overfitting the model.
339



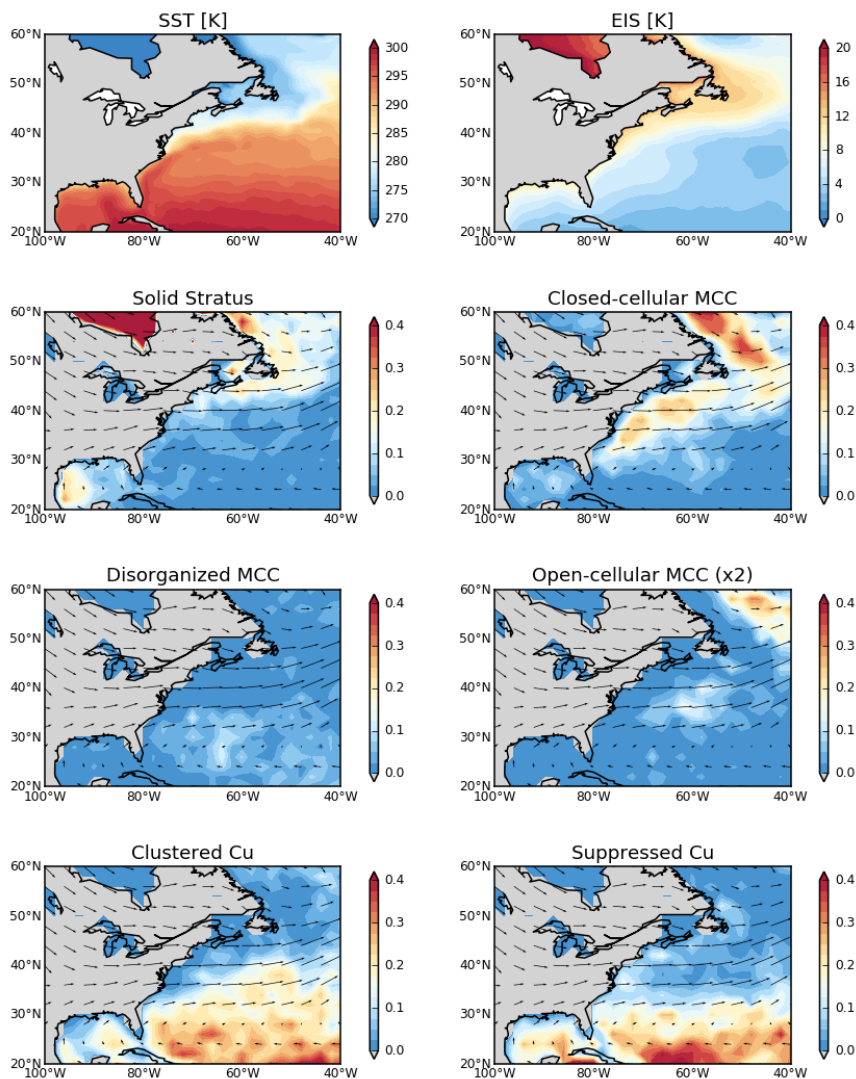
340
 341 Figure 6: Confusion matrix of the model predictions on test data.



342
 343 Figure 7: An example granule illustrating the results of the classification algorithm. This is quite
 344 a complex granule with different morphology types mixed together. The left and right margins

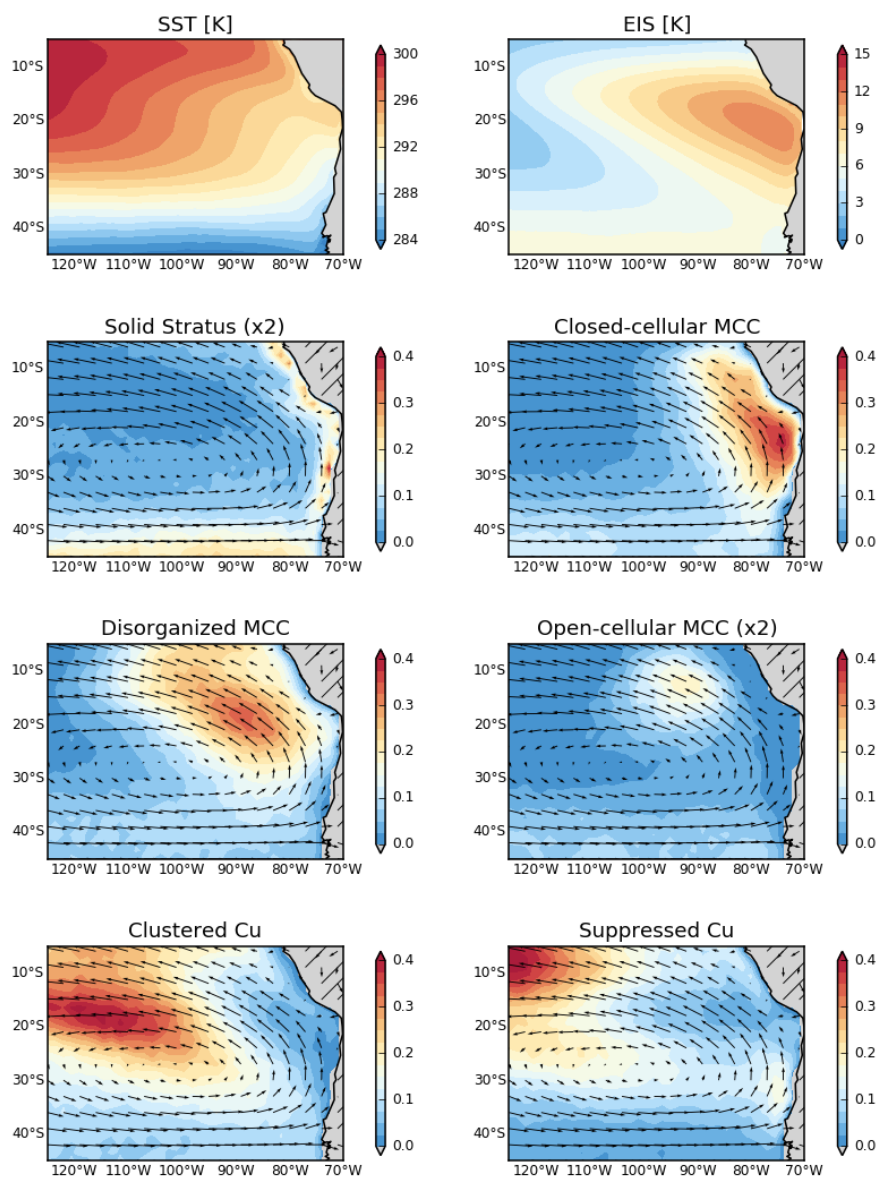


345 are not classified because current algorithm filters out scenes whose sensor viewing zenith
346 angles are greater than 45 degrees. The image is taken by NASA MODIS.
347



348
349
350
351
352
353
354
355

Figure 8: Frequency distributions of six morphology types obtained from the classification algorithm in the Northwest Atlantic region off the east coasts of US and Canada in the winter of 2011. The top two panels show the SST and EIS distributions using MERRA-2. Seasonal mean wind vectors at 850hPa are plotted to illustrate the flow. We double the values for frequency of the open-cellular type to make them numerically comparable with other types.



356
357 Figure 9: Frequency distributions of various morphology types obtained from the classification
358 algorithm in the subtropical eastern Pacific off the coast of South America for the period 2003-
359 2018. The top two panels show the SST and EIS climatology from MERRA-2 for the same period.
360 Note the doubling of scale on the stratus and open-cellular types.

361
362 **6. Author Contribution**



363 T. Y. implemented the method to train the network model. H. S., J. M., and T.Y. prepared the
364 training data. All co-authors contributed to compiling the training dataset. T. Y. wrote the
365 manuscript with contributions from other co-authors.
366

367 7. Reference

368 Agee, E. M., & Dowell, K. E. (1974). Observational Studies of Mesoscale Cellular Convection.

369 *Journal of Applied Meteorology*, 13(1), 46–53. <https://doi.org/10.1175/1520->

370 0450(1974)013<0046:OSOMCC>2.0.CO;2

371 Atkinson, B. W., & Zhang, W. J. (1996). Mesoscale shallow convection in the atmosphere.

372 *Reviews Of Geophysics*, 34(4), 403–431. <https://doi.org/10.1029/96RG02623>

373 Deng, J., Dong, W., Socher, R., Li, L.-J., Kai Li, & Li Fei-Fei. (2009). ImageNet: A large-scale

374 hierarchical image database. In *2009 IEEE Conference on Computer Vision and Pattern*

375 *Recognition* (pp. 248–255). <https://doi.org/10.1109/CVPR.2009.5206848>

376 Gelaro, R., McCarty, W., Suárez, M. J., Todling, R., Molod, A., Takacs, L., et al. (2017). The

377 Modern-Era Retrospective Analysis for Research and Applications, Version 2 (MERRA-2).

378 *Journal of Climate*, 30(14), 5419–5454. <https://doi.org/10.1175/JCLI-D-16-0758.1>

379 LeCun, Y., Bengio, Y., & Hinton, G. (2015). Deep learning. *Nature*, 521(7553), 436–444.

380 <https://doi.org/10.1038/nature14539>

381 McCoy, I. L., Wood, R., & Fletcher, J. K. (2017). Identifying Meteorological Controls on Open and

382 Closed Mesoscale Cellular Convection Associated with Marine Cold Air Outbreaks.

383 *Journal of Geophysical Research: Atmospheres*, 122(21), 11,678–11,702.

384 <https://doi.org/10.1002/2017JD027031>



- 385 Muhlbauer, A., McCoy, I. L., & Wood, R. (2014). Climatology of stratocumulus cloud
386 morphologies: microphysical properties and radiative effects. *Atmospheric Chemistry
387 And Physics*, 14(13), 6695–6716. <https://doi.org/10.5194/acp-14-6695-2014>
- 388 Platnick, S., Meyer, K. G., King, M. D., & Wind, G. (2016). The MODIS Cloud Optical and
389 Microphysical Products: Collection 6 Updates and Examples From Terra and Aqua. *Journal
390 on Geoscience and Earth System Science*. Retrieved from
391 <http://ieeexplore.ieee.org/abstract/document/7707459/>
- 392 Simonyan, K., & Zisserman, A. (2015). Very Deep Convolutional Networks for Large-Scale Image
393 Recognition. *ArXiv:1409.1556 [Cs]*. Retrieved from <http://arxiv.org/abs/1409.1556>
- 394 Stevens, B., Vali, G., Comstock, K., Wood, R., van Zanten, M. C., Austin, P. H., et al. (2005).
395 Pockets of open cells and drizzle in marine stratocumulus. *Bulletin Of The American
396 Meteorological Society*, 86(1), 51–. <https://doi.org/10.1175/BAMS-86-1-51>
- 397 Wang, H., & Feingold, G. (2009). Modeling mesoscale cellular structures and drizzle in marine
398 stratocumulus. Part I: Impact of drizzle on the formation and evolution of open cells.
399 *Journal Of The Atmospheric Sciences*, 66(11), 3237–3256.
400 <https://doi.org/10.1175/2009JAS3022.1>
- 401 Wood, R., & Bretherton, C. S. (2006). On the relationship between stratiform low cloud cover
402 and lower-tropospheric stability. *Journal Of Climate*. Retrieved from
403 <http://journals.ametsoc.org/doi/pdf/10.1175/JCLI3988.1>
- 404 Wood, Robert. (2012). Stratocumulus Clouds. *Monthly Weather Review*, 140(8), 2373–2423.
405 <https://doi.org/10.1175/MWR-D-11-00121.1>



- 406 Wood, Robert, & Hartmann, D. L. (2006). Spatial variability of liquid water path in marine low
407 cloud: The importance of mesoscale cellular convection. *Journal Of Climate*, 19(9),
408 1748–1764.
- 409 Yuan, T. (2019). Understanding Low Cloud Mesoscale Morphology with an Information
410 Maximizing Generative Adversarial Network. <https://doi.org/10.31223/osf.io/gvebt>
- 411 Yuan, T., & Oreopoulos, L. (2013). On the global character of overlap between low and high
412 clouds. *Geophysical Research Letters*, 40(19), 5320–5326.
413 <https://doi.org/10.1002/grl.50871>
414